

Heat Energy Impacts on Hybrid (Copper–Titanium/Water) Nanofluid Flow Over a Porous Elongated Sheet

B. Venkateswarlu¹, P. V. Satya Narayana^{2,*}, and Ali J. Chamkha³

This research delves into the MHD thermally radiative heat transfer of a blend of nanofluid flowing from a stretching surface, applicable to various fields such as biomedical technology, solar power systems, medical therapies, and photoelectric devices. A groundbreaking element of this exploration is the integration of temperature-sensitive viscosity in the momentum equation, along with accounting for heat source and thermal radiation in the energy equation. The basic equations governing the flow are converted into ODEs using suitable similarity parameters and then computationally solved using the R-K-F method along with shooting technique. Significant findings regarding different parameters affecting flow characteristics (i.e., $f'(\eta)$, $\theta(\eta)$, Cf, Nu) are depicted qualitatively through graphical representations. The speed and temperature of the hybrid nanofluid (Cu–TiO₂/H₂O) are observed to exceed those of the single-component nanofluid (TiO₂/H₂O) as heat generation and convection factor values increase. Moreover, the Nusselt number declines as radiation levels rise. The study infers that the heat transfer efficiency of the hybrid nanofluid surpasses that of the single component nanofluid and hence the viscous fluid. Additionally, the outcomes closely correspond with the behavior of a viscous fluid under specific conditions.

KEYWORDS: Thermal Radiation, MHD, HNFs, Variable Viscosity, Porous Medium, Stretching Sheet.

1. INTRODUCTION

Hybrid nanofluids (HNFs) involve the intricate suspension of various nanoparticles (NPs), whether in a mixture or composite form, aiming to enhance thermal conductivity and heat transfer (HT) properties in applications of thermal engineering. The exploration of HNF is currently at a nascent phase, largely due to the intricate behavior of spinning NPs and their varying chemical compositions. The problem of HT flow due to exponentially stretched/shrinking sheet was deliberated by Wahid et al.1 This study is focused on controlling the parameters for better HT in practical and industrial applications. An in-depth analysis of the thermal characteristics of hybrid nanoliquid was conducted by Sajid and Ali.² Their research uncovered that the dependability of hybrid nanoliquid is achieved by the thermal conductivity of various nanoparticle blends. Salman et al.³ explored the review of HT of HNF over

various fluid flow models. Roy4 preferred the finite difference procedure for the convective stream of HNF in a wavy surface and originates that the ratios of drag force and HT amplified with the strength of magnetic field (MF), nanofluid (NF) volume fraction and amplitude wavelength. The diverse characteristics of various nano-additives under varying models and boundary conditions were meticulously investigated through experimental and computational methods by Refs. [5-13]. Manjunatha et al. 14 delved into the intricate realm of HT properties in flows containing various nano additives influenced by a stretching sheet (SS). Hayat and Nadeem¹⁵ also explored the fascinating dynamics of HT in similar flow conditions but with a different approach. The reactions of HNFs in a permeable cylinder were examined by Ramesh et al.16 They noticed that the HNF (i.e., ND-Co₃O₄/EG) plays a new imposing role in the process of energy transfer. Ramesh et al. 17 exposed the Darcy-Forchheimer flow of HNF in a thin needle by adapting Newtonian heating. Their study is handy in modern technologies (micro scale and structure electronic and cooling gadgets) and building procedures. Recently, Adun et al.18 and Xiong et al.19 reviewed the applications of coupled NF in various thermal energy structures.

*Author to whom correspondence should be addressed.

Email: pvsatya8@yahoo.co.in Received: 18 April 2021

Revised/Accepted: 12 January 2022

¹School of Mechanical Engineering, Yeungnam University, Gyeongsan-si, 38541, Republic of Korea

²Department of Mathematics, SAS, VIT, Vellore 632014, T.N., India

³ Faculty of Engineering, Kuwait College of Science and Technology, Doha District, 35004, Kuwait

Venkateswarlu and Satya Narayana²⁰ scrutinised the MHD dissipative flow effects over SS by using the coupled NPs and they concluded that their outcomes are useful in cancer therapy, and power generation where the viscosity of fluid changes with temperature.

Magnetohydrodynamics linked with HNF flows boasts abundant efforts in the realms of industry and engineering, including plasma research, MHD power generation, aerodynamics, crystal formation, and the petroleum sector, among others. Moreover, the EMF is used in medical treatments (EMI scanning, Cancer therapy etc.). Also, an emotional and physical trouble occurred in human body is only due to an unstable EMF. Patil and Kulkarni²¹ examined the MHD HNF flow due to a slender cylinder in the presence of MF in view of various applications such as solar cells, and photo electric devices, etc. Waqas et al.²² projected the shooting scheme for MHD flow of hybrid NPs in a radially rotating disk. They ensure that the velocity flatten and temperature bust-up through well-built of MF.

Moreover, a multitude of contemporary scholars^{23–28} delved into exploring the impact of magnetohydrodynamics in combination with various nano-enhancements across diverse cavity prototypes. Ijaz Khan et al.²⁹ scrutinized the magnetic rotating flow amidst two parallel surfaces while hybrid NPs and entropy production were in play. Their observation unveiled that the heightened thermal exchange between the plates stemmed from the existence of a MF, along with Eckert and Prandtl numbers. Abbas et al.30 inspected the 3D micropolar-mixed NF in a rotating porous channel by taking the MF and convective conditions. They used bvp4c code for the solutions and found that the HT of HNFs is higher than that of NF in the light of rotation and porosity. Waini et al.31 and Emad and Pop32 numerically investigated the influence of MHD and thermal heat flux over SS in the presence of hybrid NPs. Authors33, 34 explored the convective flow of Carreau and Oldroyd-B NF along Brownian motion over a SS/cylinder by using bvcp4c algorithm. Their study mainly explored the HT of NF applications in industrial and medicinal sciences.

The thermal radiation plays a vital role in numerous industrial and aerospace settings where high temperatures are present. Lately, the fusion of thermal energy with various nanoparticle blends has captured the attention of numerous contemporary scientists. Tullius and Bayazitoglu³⁵ delved into the exploration of HNF through a meticulous radiation analysis. Within their study, the intensity of radiation was found to be intricately linked to factors such as particle density, size, container height, temperature, and concentration. Hayat et al.³⁶ delved into the enhancements in heat properties exhibited by hybrid NPs when influenced by slip effects and thermal heat. The outcome of their inquiry unveiled that the thermal diffusivity of common NFs is surpassed by that of amalgam NF. Iqbal et al.³⁷ delved into the realm of thermal radiation, utilizing closed form solutions within a vertical channel with the aid of hybrid NPs. The HNFs were crafted

using both Cu and CuO NPs, revealing that platelets play a more potent role in enhancing HT compared to brickshaped NPs. Chamkha et al.38 delved into the realm of a spinning mechanism combined with a fusion of NF using the Duan-Rach Approach. The study involved the contemplation of dual permeable and flexible plates within a rotating setup infused with Joule heating and radiation. Shoaib et al.³⁹ executed the solutions of redial and dissipative flow possessions on MHD HNF in a rotating disk by using Lobatto IIIA system and found the rate of HT coefficient is inversely proportional to the upgraded values of MF, NF volume fraction and Brinkman number. Nilankush et al.40 delved into the realm of homotopy perturbation analysis on a porous sheet impacted by radiation, delving into various nanoparticle blends. An intriguing observation emerges as magnetic strength increases, fluid velocity decreases, yet heat transport is augmented by radiation. Gireesha et al.⁴¹ creatively employed the RKF technique to analyse a HNF scenario involving a porous longitudinal fin in motion under radiation. By setting distinct conditions at the fin's tip, they determined that the HT of a fin with a identified convective quantity surpasses that of a fin with an insulated tip. Authors⁴² delved into the study of an axisymmetric HNF flow influenced by MF, radiation, and Joule heating. Their research unveiled that the MF strength increases when combined with Cu-water HNF, whereas the presence of copper leads to the decline of Eckert numbers. Influence of Jeffery-Hamel flow utilizing HNF with base fluid as ethylene glycol in a converging/diverging channel was scrutinized by Faisal et al.43 In their study, the diamond and Silica NPs are used in view of applications in medicine such as: inflammation of the lung tissue, autoimmune diseases, bronchitis and silicosis.

The essence of the current study's innovation lies in filling a void within existing research, delving into the impact of variable viscosity on HNFs. Variable viscosity plays a pivotal role in various cooling mechanisms, fluctuating alongside temperature based on the nanoparticle blends utilized. Acknowledging this significance, our investigation computationally dissects the MHD radiative HT of Copper-Titanium/water HNFs featuring a heat source and variable viscosity. The examination is executed utilizing the RKF approach in conjunction with the shooting method, a resilient numerical technique for resolving differential equations. By integrating variable viscosity, this exploration offers a more precise and authentic representation of the thermal dynamics of HNFs, furnishing valuable perspectives to the realm of heat conduction and cooling innovations.

2. MATHEMATICAL MODELING

The exploration at hand delves into the intricate realm of two-dimensional steady-state electromagnetic and thermally radiated fluid dynamics approaching a porous SS,

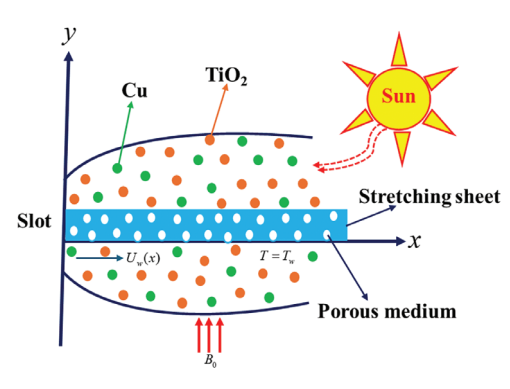


Fig. 1. The model depicting the physical flow.

under the influence of a heat source, utilizing a Copper-Titanium/water HNF. Exhibited in Figure 1 is the concrete model's physical representation linked to this specific instance. Within this structure, the liquid elegantly adheres to the *x*-axis, but the *y*-axis is upright to it. Central to this examination is the pivotal assumption that the fluid's viscosity is a variable entity, subject to changes in temperature. This fluctuation holds immense relevance as it exerts a profound impact on the fluid's conduct and thermal transmission properties. Through the integration of variable viscosity effects, the primary objective of this investigation is to furnish a profound insight into the intricate dynamics and thermal efficacy of the HNF during electromagnetic fields and thermal irradiation.

The primary formulas governing the flow of mixed NF are precisely outlined as: 14,44

$$u_x + v_y = 0$$

$$\rho_{\text{hnf}} \left\{ u u_x + v u_y \right\}$$

$$= \frac{\partial}{\partial y} \left\{ \mu_{\text{hnf}}(T) u_x \right\} + g(T - T_{\infty}) (\beta \rho)_{\text{hnf}}$$

$$- \left\{ \sigma B_0^2 + \frac{\nu_f}{K^*} \right\} u$$
(2)

$$(\rho c_p)_{\rm hnf} \left\{ u \, T_x + v \, T_y \right\} = k_{\rm hnf} \frac{\partial^2}{\partial y} (T) - \frac{\partial}{\partial y} (q_r^*) + Q_H (T - T_\infty)$$
(3)

The limits of the system are outlined in the following: $^{14, 15, 45}$

At
$$y = 0$$
: $u = u_w(x) = ax$, $v = 0 = T - T_w$
As $y \to \infty$: $u \to 0$, $T - T_\infty \to 0$ (4)

The fundamental characteristics of NPs and the primary fluid are elucidated (at 250 $^{\circ}$ C) in Table I as follows. $^{14,\,15,24,\,46}$

The intriguing thermophysical properties exhibited by NFs and the groundbreaking nature of HNFs are outlined below.

Viscosity:
$$\mu_{nf} = \mu_f \sqrt{(1 - \phi_1)^5} \\ \mu_{hnf} = \mu_f \sqrt{\{(1 - \phi_1)(1 - \phi_2)\}^5}$$
 (5)

Table I. The characteristics of NPs in conjunction with the base fluid.

Properties	Cu	TiO ₂	H_2O
$\beta \times 10^5$ (1/K): thermal expansion coefficient	1.65	-	21
k_f (W/m K): thermal conductivity	400	8.4	0.6071
Cp (J/K): heat Capacity	385	692	4179
ρ (kgm ⁻³): density	8933	4175	997.1

Density:
$$\begin{aligned}
\rho_{nf} &= \rho_f (1 - \phi_1) + \phi_1 \rho_{s1} \\
\rho_{hnf} &= \rho_f (1 - \phi_1) (1 - \phi_2) \\
&+ (1 - \phi_2) \phi_1 \rho_{s1} + \phi_2 \rho_{s2}
\end{aligned} (6)$$

Thermal expansion coefficient:

$$\beta_{nf} = \beta_{f}(1 - \phi_{1}) + \phi_{1}\rho_{s1}
\beta_{hnf} = \beta_{f}(1 - \phi_{1} - \phi_{2} + \phi_{1}\phi_{2})
+ (1 - \phi_{2})(\phi\beta_{s})_{1} + (\phi\beta_{s})_{2}$$
(7)

Heat capacity:

$$(\rho c_{p})_{nf} = (\rho c_{p})_{f} - \phi_{1}(\rho c_{p})_{f} + (\rho c_{p}\phi)_{s1}$$

$$(\rho c_{p})_{hnf} = (1 - \phi_{1} - \phi_{2} + \phi_{1}\phi_{2})(\rho c_{p})_{f}$$

$$+ (1 - \phi_{2})(\rho c_{p}\phi)_{s1} + (\rho c_{p}\phi)_{s2}$$
(8)

Sci Thermal conductivity:

$$k_{nf} = \left(\frac{k_{s1} + (n-1)\left\{(1 - \phi_1)k_f + \phi_1 k_{s1}\right\}}{k_{s1} + (n-1 + \phi_1)k_f - \phi_1 k_{s1}}\right) k_f$$

$$k_{\text{hnf}} = \left(\frac{k_{s2} + (n-1)\left\{(1 - \phi_2)k_{nf} + \phi_2 k_{s2}\right\}\right\}}{k_{s2} + (n-1 + \phi_2)k_{nf} - \phi_2 k_{s1}}\right) k_{nf}$$
(9)

The radiative heat flux q_r^* can be described by employing the Rosseland approximation for radiative HT, which is defined as follows:^{47, 48}

$$q_r^* + \left(\frac{4\sigma^*}{3k^*} \times \frac{\partial T^4}{\partial y}\right) = 0 \tag{10}$$

The fluctuations in temperature of the flow term T^4 are depicted in Taylor's series in a unique form:

$$T^4 \approx \{4T - 3T_\infty\} \times T_\infty^3 \tag{11}$$

Table II. Comparison of C_f .

		Drage force				
	Ref.	[14]	Curren	t study		
M	NF	HNF	NF	HNF		
0.5	0.5779 0.6915	0.5865 0.7199	0.57795 0.69152	0.58654 0.71997		
1.5	0.7982 0.8994	0.8422 0.9549	0.79827 0.89948	0.84229 0.95494		

Table III.	Comparison	of Nu.					
		Nusselt number					
	Ref. [14]		Curren	t study			
Pr	NF	HNF	NF	HNF			
1.5	0.2002	0.2021	0.2005	0.20214			
3	0.2004	0.2042	0.20056	0.20429			
4.5	0.2006	0.2063	0.20067	0.20637			
6	0.2008	0.2084	0.20089	0.20849			

The simplification of Eq. (2) is smoothly accomplished with the direction from Eqs. (10) and (11) in the following way:

$$(\rho c_p)_{\text{hnf}} \left\{ u \frac{\partial u}{\partial x} + v \frac{\partial u}{\partial y} \right\}$$

$$= \left\{ k_{\text{hnf}} + \frac{16\sigma^*}{3k^*} \times T_{\infty}^3 \right\} \frac{\partial^2 T}{\partial y} + Q_H (T - T_{\infty}) \quad (12)$$

The consideration of fluid flow viscosity should include the temperature dependency in the following:¹⁴

$$\mu_f = \mu_0 \times e^{-B\,\theta(\eta)} \tag{13}$$

The present investigation introduces innovative similarity transformations aimed at tackling the complex two-dimensional dynamics of steady electromagnetic and thermally radiated fluid motion towards a porous SS in the context of a Copper-Titanium/water HNF. These profound transformations are elegantly articulated as follows: 14, 45

$$\eta = \sqrt{\frac{a}{\nu_f}} y, \quad \theta(\eta) = \frac{T - T_\infty}{T_w - T_\infty},
v = -f(\eta) \sqrt{a\nu_f}, \quad u = a x f'(\eta)$$
(14)

By utilizing the formula of similarity transformations in Eq. (14) in conjunction with Eq. (4), the expressions (2) and (12) manifest themselves in the subsequent configurations.

$$f''' - Bf''\theta' + \delta_1 \left\{ \delta_2(ff'') - f'^2 - \left(M + \frac{1}{K}\right)f' + \delta_2\delta_3\lambda\theta \right\} = 0$$
 (15)

$$\left\{ \delta_4 + \frac{4}{3}R \right\} \theta'' + \Pr\{\delta_5 f \theta' + Q \theta\} = 0$$
 (16)

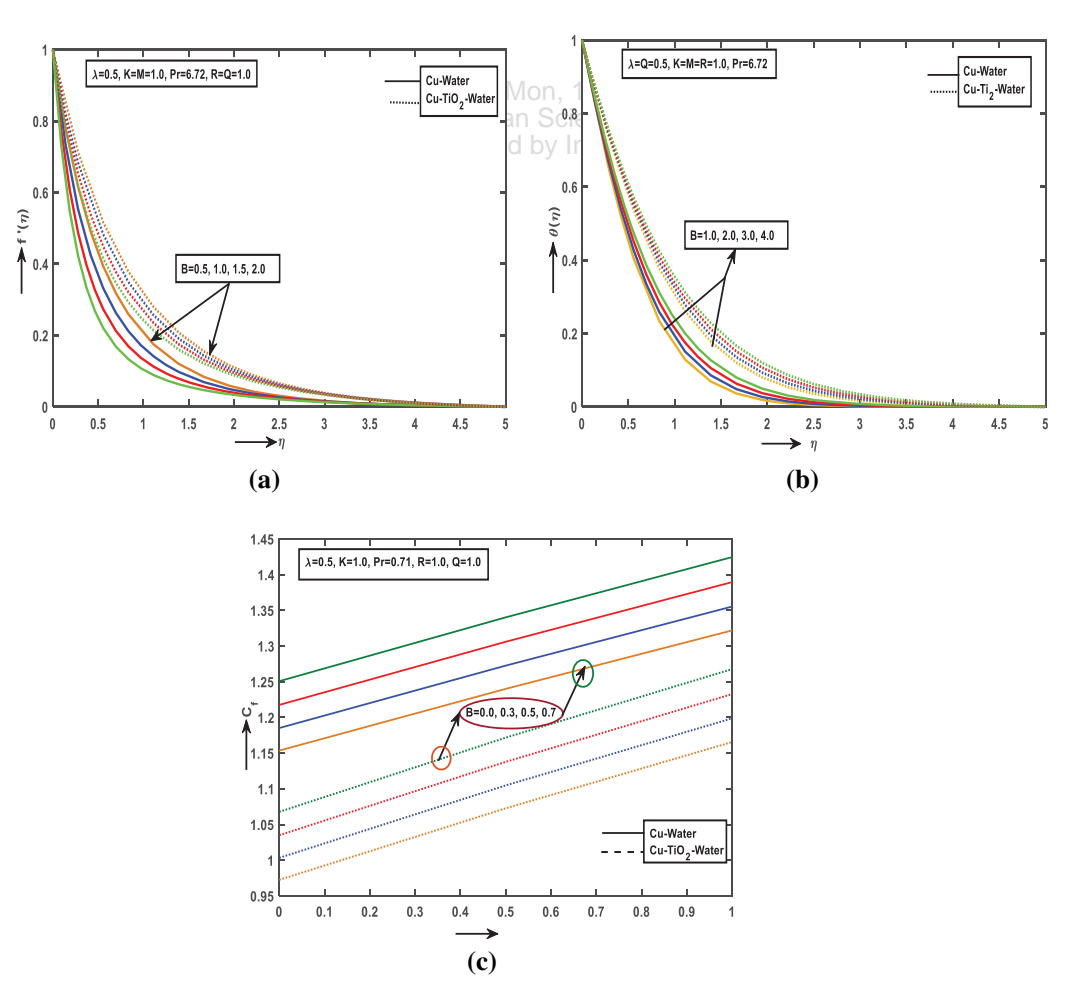


Fig. 2. The impact of B on (a) speed, (b) temperature patterns and (c) surface friction.

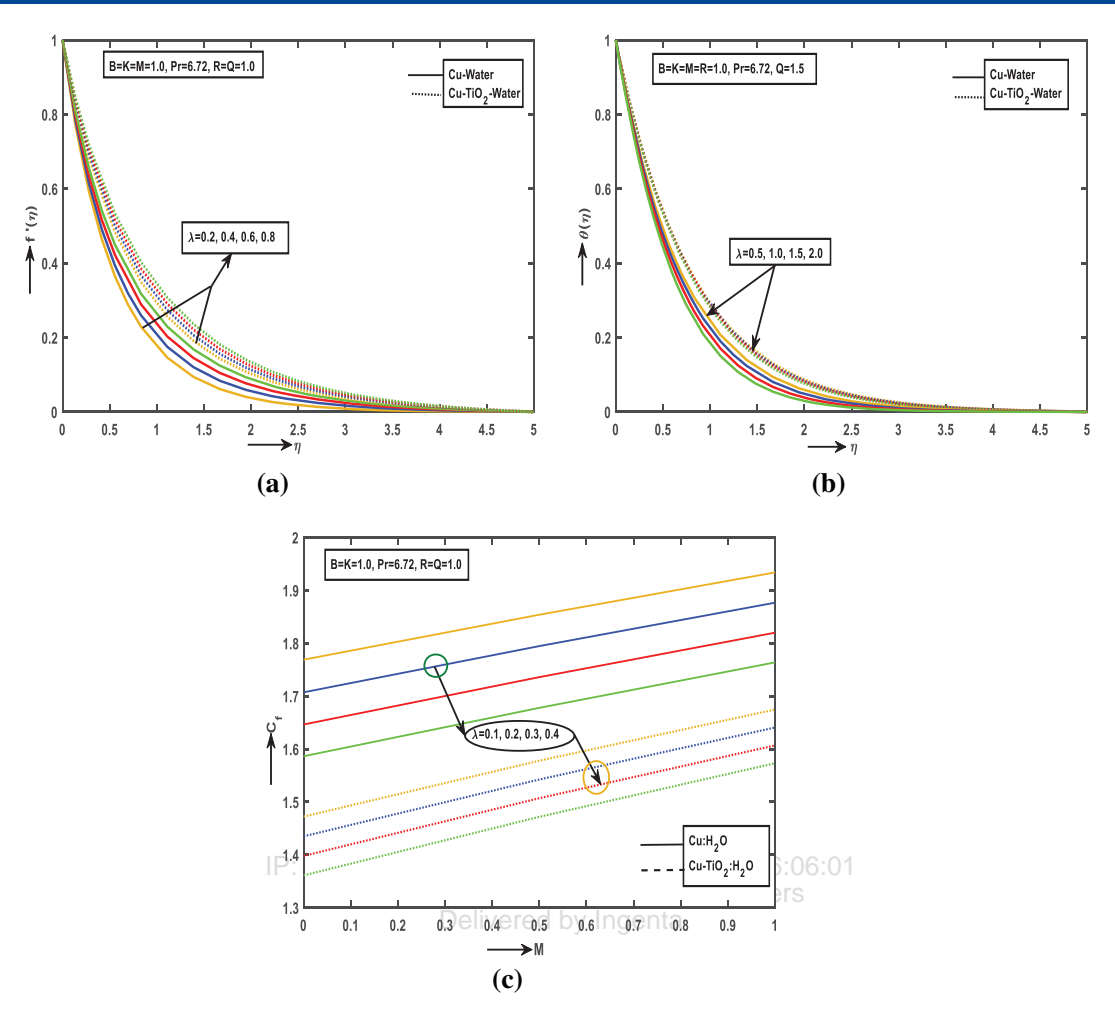


Fig. 3. The convection factor impacts the (a) speed, (b) heat distribution, and (c) resistance at the surface.

The BCs that correspond are undergoing a transformation in the following:

At
$$\eta = 0$$
: $f = 0$, $f' = 1 = \theta$
As $\eta \to \infty$: $f' = 0 = \theta$ (17)

where $K = aK^*(\rho/\nu)_f$, $\lambda = (g\beta_f/a u_w) \times \Delta T$, $M = \sigma B_0^2/a\rho_f$, $\text{Pr} = (\nu/k)_f \times (\rho c_p)_f$, $R = (4\sigma^*T_\infty^3)/(k^*k_f)$, $Q = Q_H/a(\rho c p)_f$.

3. PHYSICAL ASPECTS

The coefficient of drag on the surface and the Nusselt number are elegantly represented by the following expressions:^{14,49}

$$C_f = \left(\frac{\mu_{\text{hnf}}}{\rho_f u_w^2}\right) \times \left(\frac{\partial u}{\partial y}\right)_{y=0} \Rightarrow \sqrt{\text{Re}_x} \times C_f = \frac{1}{\delta_1} \times f''(0)$$
(18)

$$Nu = -\left(\frac{x \, k_{\text{hnf}}}{k_f \Delta T}\right) \times \left(\frac{\partial T}{\partial y}\right)_{y=0} \Rightarrow \frac{Nu}{\sqrt{\text{Re}_x}} = -\delta_4 \times \theta'(0) \tag{19}$$

where $\text{Re}_x = x u_w / v_f$ is the Reynolds number.

4. RESULTS VALIDATION

Tables II and III exhibit the validity of present work with Manjunatha et al.¹⁴ and reviled that the existing results are meticulously matched with Ref. [14] as a limiting case. Table II: Evaluating the relationship between skin-friction and HT ratio in the current scenario compared to the study by Manjunatha et al.¹⁴ considering various parameters such as $\lambda = 1 = B$ and Pr = 6.72 at $K \to \infty$ and R = Q = 0.

5. RESULTS AND DISCUSSION

The purpose of this department is to investigate the influence of different physical factors such as: variable viscosity, convention, porous permeability, MF, radiation and heat source factors and Prandtl number, in the presence of Copper-Titanium oxide-water hybrid and mono NF phase on fluid flow through Figures 2–8. In these calculation processes, the parameter values are varied over a range which are listed in the corresponding figure legends.

Figures 2(a)–(c) showcase how the flow, temperature, and surface drag coefficient are impacted by the variable viscosity parameter (*B*) in different scenarios of Cu–TiO₂:H₂O and Cu:H₂O. The fluid's velocity slows

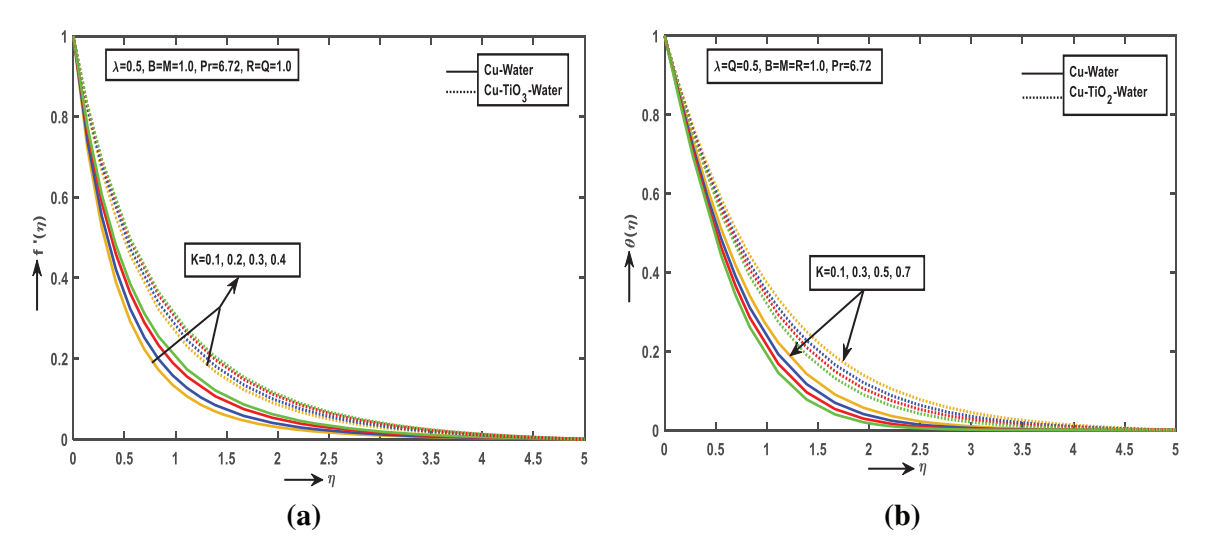


Fig. 4. The influence of (a) speed and (b) heat patterns concerning K.

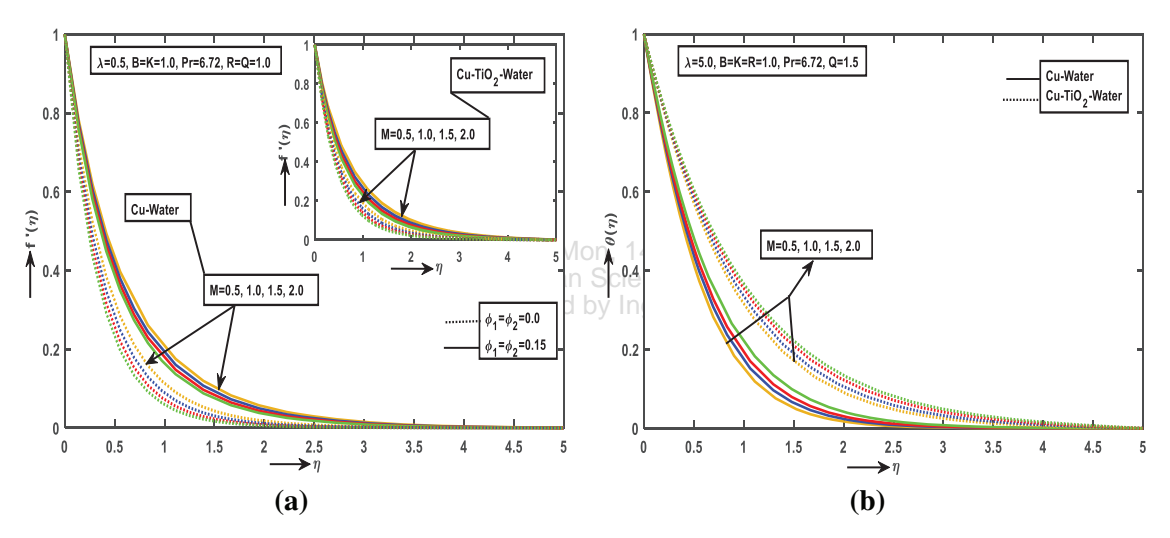


Fig. 5. The influence of (a) speed and (b) heat distribution in connection to M.

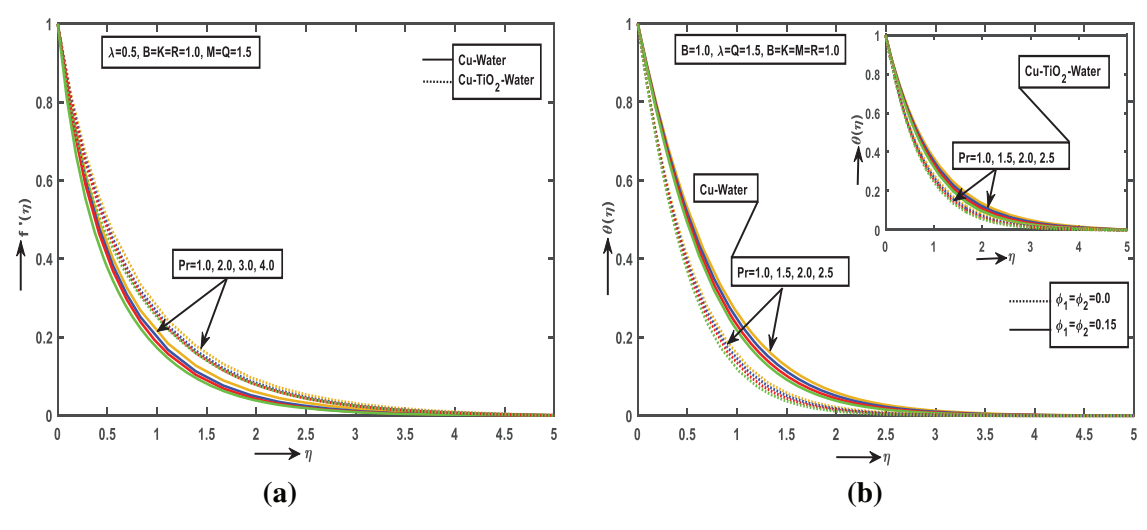


Fig. 6. The influence of (a) speed and (b) heat patterns concerning Pr.

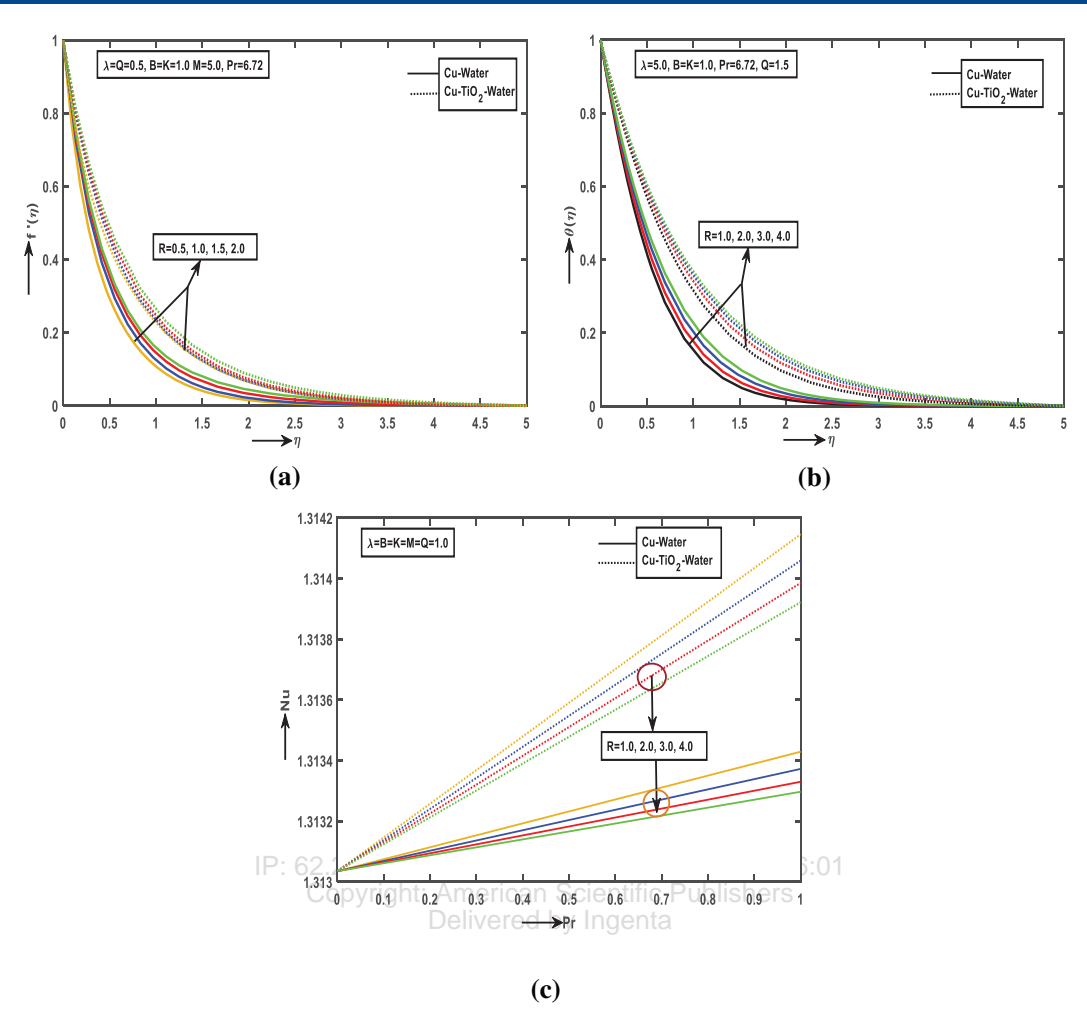


Fig. 7. The influence of (a) velocity, (b) temperature profiles and (c) Nu with respect to R.

down as it moves across the SS, while the temperature and surface drag coefficient rise with an increase in *B*. Notably, the copper-titanium/water NF exhibits higher velocity and temperature compared to the Cu:H₂O NF. The fluid's viscosity decreases physically as *B* value rises, leading to a reduction in velocity. Furthermore, the Cu:H₂O NF achieves the boundary more quickly than the Cu-TiO₂:H₂O HNF because of temperature-responsive viscosity. Furthermore, the HNFs temperature exceeds that of the copper-water NF due to its reduced viscosity. However, this pattern reverses when considering the surface drag coefficient.

The variations in the convection factor (λ) impact velocity, temperature, and skin friction as illustrated in Figures 3(a)–(c). A rise in λ results in an augmented velocity profile. With increasing λ , the fluid velocity is boosted due to the potency of buoyancy. The buoyancy force, acting as a beneficial pressure gradient, propels the flow upwards, leading to an escalation in velocity. Conversely, the temperature and surface drag coefficient of the fluid diminish as λ increases. This can be attributed to the widening gap between the surface and ambient

temperatures at higher λ values. Contrary to the Cu-water NF, the Cu-TiO₂:H₂O HNF reveals higher velocity and temperature, while displaying the reverse trend for the C_f .

The distribution of flow and temperature as a function of η for various permeability parameter (K) values is explored in Figures 4(a) and (b) using copper/H₂O NF and copper-TiO₂/water composite NF. The velocity of the combined fluid rises as K values increase, while the impact on temperature is the opposite. The sheet's porosity grows with higher K values, leading to an escalation in fluid velocity. Indisputably, the temperature of the HNF exceeds that of the mono NF.

The different values of the MF parameter (M) showcase the variations of $f'(\eta)$ and $\theta(\eta)$ against η in Figures 5(a) and (b), respectively. It becomes apparent that $f'(\eta)$ experiences a decline while $\theta(\eta)$ shows an increase for various M values. Incredibly, the velocity of the HNF ($\phi_1 = \phi_2 = 0.15$) overtakes that of the viscous fluid and Cu-water NF. This showcases the exceptional efficiency of HNFs in contrast to standard viscous fluids and NFs. From a physical perspective, the existence of Lorentz forces results in a decline in fluid speed by counteracting its movement.

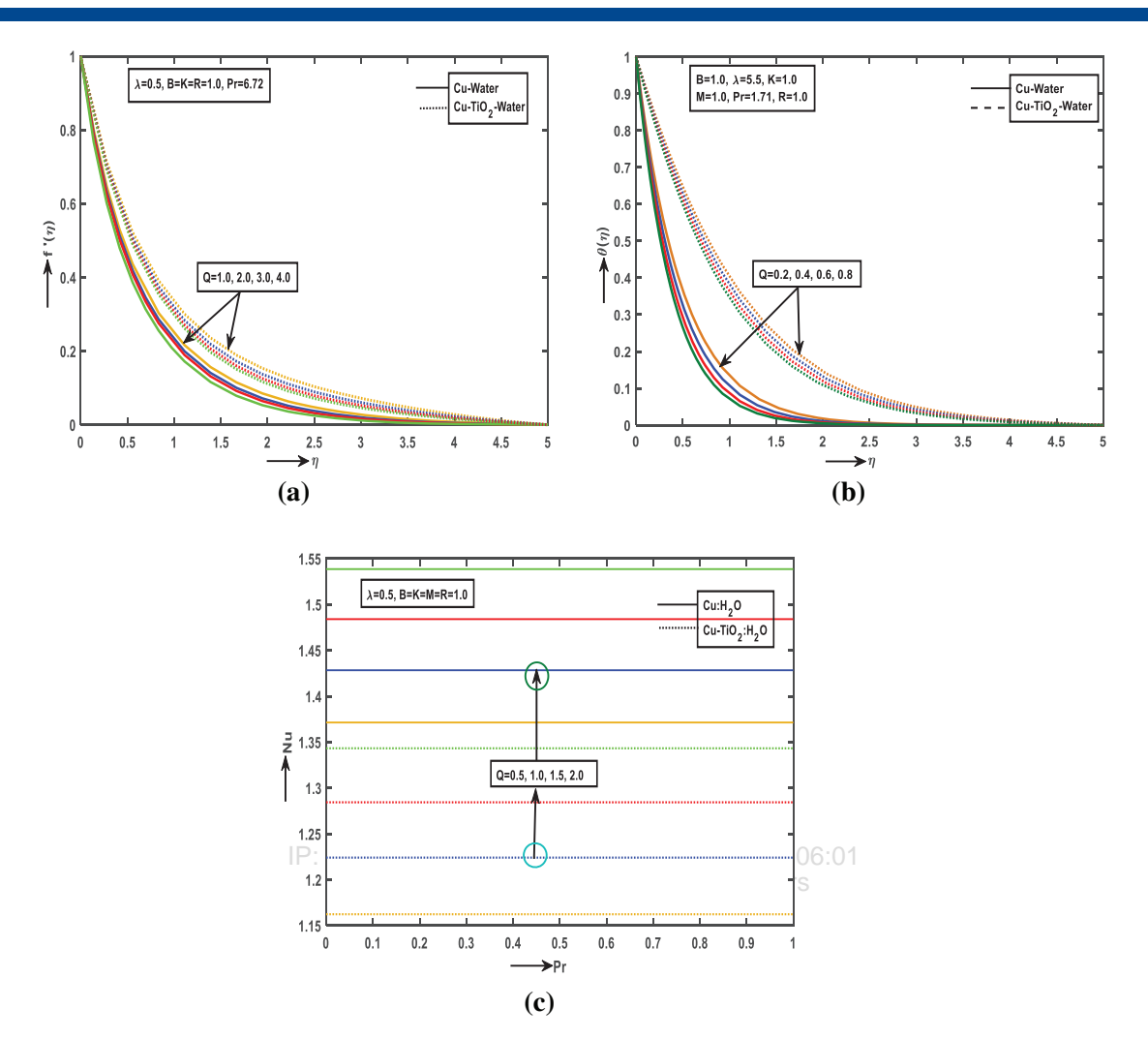


Fig. 8. The influence of (a) speed and (b) heat patterns along with (c) Nu concerning Q.

Furthermore, higher values of the volume fraction factor result in an escalation of the liquid velocity.

In Figures 6(a) and (b), one could identify a clear connection between the fluid's motion and its thermal state, demonstrating a compelling reverse correlation with the increasing Pr. Strangely, the thermal capacity of the liquid is seen to be noticeably elevated in the presence of a HNF when compared to a viscous fluid and a mono NF. On a physical level, the thermal deviating of the liquid tends to decrease with higher Pr values, ultimately leading to the formation of a narrower thermal BL. In cases where Pr exceeds 1 by a large margin, the predominant mode of HT within the fluid is predominantly through convection, owing to the superiority of motion outward over thermal deviating.

Figures 7(a)–(c) demonstrate the unique traits of $f'(\eta)$, $\theta(\eta)$, and the HT speed across different R values when exposed to diverse NF compositions. The flow and heat measure of the double NF increase with rise of R. These results also disclose that the double NF speed and temperature intensifies when radiation factor rises. Moreover,

the thermal boundary layer thicknesses are continuously magnified only when R expands and the mean absorption coefficient decays. The Nusselt number exhibits a decline as accumulative R increase. Furthermore, the hybrid phase demonstrates a higher rate of HT compared to the nano phase. Such findings hold great significance in various industrial and technical applications that involve intense HT processes.

Figures 8(a)–(c) display the deviations in $f'(\eta)$, $\theta(\eta)$, and Nu for different positive Q values. The outcomes indicate a reduction in the intensity of the momentum and temperature profiles as Nu escalates with increased Q values. Furthermore, the HNF displays superior momentum and thermal conduction in comparison to the mono NF. On the contrary, the scenario is opposite for Nu.

6. CONCLUSION

The impact of heat radiation and viscosity that changes with temperature on the flow of magnetohydrodynamic due to SS in the presence of a HNF (Cu-TiO₂:H₂O) is

examined through the application of a shooting method. The results of this study reveal significant findings.

- The speed of the liquid when combined with Cu-TiO₂ NPs surpasses that of the NF made of Copper-water for various levels of M, Q, B, Pr, and R.
- The pure fluid's temperature is relatively decreased when contrasted with the HNFs temperature over a range of Pr values.
- The surface drag force coefficient rises with accumulative M.
- The rate of HT upsurges with mounting Q and declines with growing R.
- The influence of double NF surpasses that of regular NF across all temperature distribution patterns.

NOMANCLATURE

- B_0 Magnetic field
- B Vaiable viscosity factor
- C_f Skin friction
- c_p Specific heat capacity
- g Acceleration due to gravity
- k Thermal conducitiy
- K Porous medium parameter
- k* Mean absorption coefficient
- M Magnetic field parameter
- *n* Nanoparticle size
- Nu Nusselt number
- Pr Prandtl number
- Q Heat generation factor
- q_r^* Radiative heat flux
- T Liquid temperature
- u_{w} Stretching sheet velocity
- (u, v) Speed components
- (x, y) Coordinate axes

Greek symbols

- λ Convention parameter
- β Thermal expansion
- ρ Density
- μ Viscosity
- σ Electrical conductivity
- σ^* Stephen Boltzmann constant
- ϕ_1 Alumina volume fraction
- ϕ_2 Copper volume fraction

Subscript

- f Fluid
- s Solid
- nf Nanofluid
- hnf Hybrid nanofluid
- S1 Alumina
- S2 Copper
- w Condition at the wall
- ∞ Condition at free stream

Appendix

$$\delta_1 = \frac{\mu_{\text{hnf}}}{\mu_f} = 1\sqrt{\{(1 - \phi_1)(1 - \phi_2)\}^5}$$

$$\delta_2 = \rho_{\text{hnf}}(\rho_f)^{-1} = 1 - \phi_1 - \phi_2 + \phi_1 \phi_2 + (1 - \phi_2)(\phi \rho_s)_1 / \rho_f + (\phi \rho_s)_2 / \rho_f$$

$$\delta_3 = \beta_{hnf}(\beta_f)^{-1} = 1 - \phi_1 - \phi_2 + \phi_1 \phi_2 + (1 - \phi_2)(\phi \beta_s)_1 / \beta_f + (\phi \beta_s)_2 / \beta_f$$

$$\delta_4 = k_{\rm hnf}(k_f)^{-1}$$
, where

$$\frac{k_{nf}}{k_f} = \frac{k_{s1} + (n-1)\left\{k_f - \phi_1 k_f + \phi_1 k_{s1}\right\}}{k_{s1} + (n-1+\phi_1)k_f - \phi_1 k_{s1}} \text{ and}$$

$$\frac{k_{\text{hnf}}}{k_{nf}} = \frac{k_{s2} + \left\{k_{nf} - \phi_2 k_{nf} + \phi_2 k_{s2}\right\} (n-1)}{k_{s2} + (n-1+\phi_2)k_{nf} - \phi_2 k_{s1}}$$

$$\delta_5 = (\rho C p)_{\text{hnf}} ((\rho C p)_f)^{-1}$$

$$= 1 - \phi_1 - \phi_2 + \phi_1 \phi_2 + (1 - \phi_2) (\phi (\rho C p)_s)_1 / (\rho C p)_f$$

$$+ (\phi (\rho C p)_s)_2 / (\rho C p)_f$$

References and Notes

- 1. N. S. Wahid, N. M. Arifin, N. S. Khashi'ie, I. Pop, N. Bachok, and M. E. H. Hafidzuddin, Case Stud. Therm. Eng. 25, 100982 (2021).
- P: 62.215.193.29 On: Mon. 2. M. U. Sajid and H. M. Ali, Int. J. Heat Mass Transf. 126, 211 (2018).
 - Copyright: American S. Salman, A. R. A. Talib, S. Saadon, and M. T. H. Sultan, Power Delivered by In Technol. Eng. 303, 440 (2020).
 4. N. C. Roy, Case Stud. Therm. Eng. 17, 101215 (2021). Technol. Eng. 363, 448 (2020).

 - 5. D. Madhesh, R. Parameshwaran, and S. Kalaiselvam, Exp. Therm Fluid Sci. 52, 104 (2014).
 - 6. L. S. Sundar, M. K. Singh, M. C. Ferro, and A. C. M. Sousa, Int. Commun. Heat Mass Transf. 84, 1 (2017).
 - 7. M. Afrand, D. Toghraie, and B. Ruhani, Exp. Therm. Fluid Sci. 77, 38 (2016).
 - 8. S. S. Harandi, A. Karimipour, M. Afrand, M. Akbari, and A. D'Orazio, Int. Commun. Heat Mass Transf. 26, 171 (2016).
 - 9. E. M. Hemmat, M. Afrand, S. H. Rostamian, and D. Toghraie, Exp. Therm. Fluid Sci. 80, 384 (2017).
 - 10. A. Afshari, M. Akbari, D. Toghraie, and M. E. Yazdi, J. Therm. Anal. Calorim. 132, 1001 (2018).
 - 11. A. A. Ali Akbar and P. Farhad, Heat Mass Transfer. 55, 2329 (2019).
 - 12. D. Asirinaidu, K. Ramji, and S. V. Naidu, J. Nanofluids 11, 58 (2022).
 - 13. L. S. Sundar, S. Mesfin, Y. T. Sintie, V. Punnaiah, A. J. Chamkha, and C. M. Sousa, J. Nanofluids 11, 147 (2021).
 - 14. S. Manjunatha, B. Ammani Kuttan, S. Jayanthi, A. Chamkha, and B. J. Gireesha, Heliyon 5, e01469 (1-16) (2019).
 - 15. T. Hayat and S. Nadeem, Results Phys. 7, 2317 (2017).
 - 16. G. K. Ramesh, M. Manjunatha, G. S. Roopa, and A. J. Chamkha, J. Therm. Anal. Calorim. 146, 1 (2020).
 - 17. G. K. Ramesh, S. A. Shehzad, and M. Izadi, Arab. J. Sci. Eng. 45, 9569 (2020).
 - 18. H. Adun, I. W. Osho, E. C. Okonkwo, D. Kavaz, and M. Dagbasi, J. Mol. Liq. 340, 1 (2021).
 - 19. Q. Xiong, S. Altnji, T. Tayebi, M. Izadi, A. Hajjar, B. Sunden, and L. K. B. Li, Sustain. Energy Technol. Assess. 47, 101341 (2021).
 - 20. B. Venkateswarlu and P. V. Satya Narayana, Heat Transf. 50, 432 (2021)
 - 21. P. M. Patil and M. Kulkarni, Chin. J. Phys. 73, 406 (2021).

- H. Waqas, U. Farooq, R. Naseem, S. Hussain, and M. Alghamdi, Case Stud. Therm. Eng. 26, 101015 (2021).
- S. Hussain, S. E. Ahmed, and T. Akbar, Int. J. Heat Mass Transf. 114, 1054 (2017).
- 24. H. R. Ashirynejad and A. Shahriari, Results Phys. 9, 440 (2018).
- M. A. Mansour, S. Siddiqa, G. R. Subba Reddy, and A. M. Rashad, Therm. Sci. Eng. Prog. 26, 57 (2018).
- S. O. Giwa, M. Sharifpur, and J. P. Meyer, *Int. J. Heat Mass Transf.* 148, 119072 (2020).
- 27. T. Barman, S. Roy, and A. J. Chamkha, J. Nanofluids 11, 142 (2022).
- N. I. Kamis, L. Y. Jiann, S. Shafie, T. K. A. Khairuddin, and M. F. Md Basir, J. Nanofluids 11, 142 (2022).
- M. Ijaz Khan, M. U. Hafeez, T. Hayat, M. Imran Khan, and A. Alsaedi, Comput. Methods Programs Biomed. 183, 105093 (2020).
- S. Z. Abbas, W. A. Khan, M. M. Gulzar, T. Hayat, and M. Waqas, Comput. Methods Programs Biomed. 189, 105324 (2020).
- 31. I. Waini, A. Ishak, and I. Pop, J. Appl. Math. Mech. 41, 507 (2020).
- 32. H. A. Emad and I. Pop, Power Technol. 367, 192 (2020).
- 33. M. Irfan, Surf. Interfaces 23 100926 (2021).
- 34. M. Irfan, R. Aftab, and M. Khan, Chin. J. Phys. 71, 444 (2021).
- T. K. Tullius and Y. Bayazitoglu, Numer. Heat Transf. B. Fundam. 69, 271 (2016).
- 36. T. Hayat, S. Nadeem, and A. U. Khana, Eur. Phys. J. E 41, 1 (2018).
- Z. Iqbal, N. S. Akbar, E. Azhar, and E. N. Maraj, *Alex. Eng. J.* 57, 1943 (2018).

- A. J. Chamkha, A. S. Dogonchi, and D. D. Ganji, AIP Adv. 9, 025103 (2019).
- M. Shoaib, M. A. Z. Raja, M. T. Sabir, M. Awais, S. Islam, Z. Shah, and P. Kumar, *Alex. Eng. J.* 60, 3605 (2021).
- Nilankush, B. Raju, and K. Prabir Kumar, *Appl. Nanosci.* 10, 1679 (2019).
- B. J. Gireesha, G. Sowmya, M. Ijaz Khan, and H. F. Oztop, Comput. Methods Programs Biomed. 185, 105166 (2020).
- N. S. Khashi'ie, N. M. Arifin, R. Nazar, E. H. Hafidzuddin, and I. Pop, *Chin. J. Phys.* 64, 251 (2020).
- M. F. M. Basir, F. Mabood, P. V. Satya Narayana, B. Venkateswarlu, and A. I. M. Ismail, J. Therm. Anal. Calorim. 147, 661 (2020).
- 44. I. Waini, A. Ishak, and I. Pop, Int. J. Numer. Methods Heat Fluid Flow 29, 3110 (2019).
- W. A. Khan and I. Pop, Int. J. Heat Mass Transf. 53, 2477 (2010).
- S. S. Ghadikolaei, M. Yassari, H. Sadeghi, K. Hosseinzadeh, and D. D. Ganji, *Power Technol.* 322, 428 (2017).
- P. V. Satya Narayana, B. Venkateswarlu, and S. Venkataramana, Heat Transf. Asian Res. 44, 1 (2015).
- D. Harish Babu, K. A. Ajmath, B. Venkateswarlu, and P. V. Satya Narayana, J. Nanofluids 8, 1085 (2018).
- B. Venkateswarlu, P. V. Satya Narayana, and N. Taraka Ramu, *Trans. A. Razmadze Math. Inst.* 172, 619 (2018).

IP: 62.215.193.29 On: Mon, 14 Oct 2024 06:06:01 Copyright: American Scientific Publishers Delivered by Ingenta